Rapid deformation of thin gold layers in polymer matrices studied by x-ray reflectivity

Kwanwoo Shin[a)]
Department of Materials Science and Engineering, Kwangju Institute of Science and Technology, 500-712, Gwang-ju, Korea

Howard Wang,[b)] Sushil K. Satija, Charles C. Han, Daniel Josell, and John E. Bonevich
National Institute of Standards and Technology, 100 Bureau Dr., Gaithersburg, Maryland 20899

(Received 4 December 2002; accepted 21 May 2003)

We have used x-ray reflectivity to measure the morphological profiles of thin Au layers of three different average thicknesses sandwiched between two polystyrene layers with different molecular weights. The results showed that the equilibrium structures of the samples with the layers less than 4 nm thick, where discontinuous islands are expected, were very close to those of the nonannealed samples. However, the morphologies of samples with layers more than 4 nm thick, where a continuous layer structure was formed, were influenced by annealing. Comparison of transmission electron micrographs from unannealed and annealed samples showed that annealing promotes spherical shapes for the Au particles and breakup of an elongated, randomly connected structure visible prior to the annealing. The fractional area covered with Au obtained from transmission electron microscopy images is in good agreement with x-ray reflectivity results. These results were interpreted in terms of capillarity induced spheroidization of the ultrathin Au layers. © *2003 American Institute of Physics.* [DOI: 10.1063/1.1591414]

I. INTRODUCTION

Metal nanoparticles have been extensively studied because of their unique optical, magnetic and electronic properties.[1–3] The desire to develop metal/polymer nanocomposites tailored for particular applications has generated interest in the characterization of metal nanoparticles on polymer substrates.[4–6] Polymers are often used in thin film geometries in such applications as low-*k* dielectric interlayers, insulators and adhesives of fabricated metallic structures in integrated applications.[7,8] However, the substantial differences in the physical properties of these materials frequently cause unexpected problems; this is particularly true of their interfacial properties (i.e., weak adhesion, cracking or distortion), which negatively impact device density and performance in integrated circuits.[9] Understanding of the metal/polymer interface is also important for fundamental issues including dewetting,[10] diffusion,[11] and surface wave spectra.[12]

Numerous studies have focused on the behavior of thermally evaporated metallic particles on polymer substrates and shown that the physical properties at the metal/polymer interface are complex.[4,11–19] When the metallic particles are placed on the polymer surface, the deposited metals exhibit a strong clustering tendency that is characterized by nucleation, growth and coalescence. This typically results in segregation of metals on the polymer surface through the formation of large particles.[13–16] The evolution of these particles can also be influenced by the presence of air/polymer interface(s). For example, when such systems are heated above the glass transition temperature of the polymer substrate, the assembled noble metal clusters tend to diffuse into the polymer substrate.[14,15] In this case, the total free energy associated with the various interfaces acts as the driving force for the phenomena. The morphological evolution of such metallized polymer composites during annealing is expected to be a function of the average metal layer thickness, or, more specifically, the average metallic particle size and interparticle spacing. However, such evolution has not been quantitatively investigated.

Many groups have employed gold nanoparticles in a polymer matrix as markers to increase the contrast between two chemically identical polymer layers.[14,17,18] When distributed sparsely at the interface of two polymer layers, such particles permit the interdiffusion dynamics of the polymer layers to be monitored. For such applications the interaction of the noble nanoparticles with the polymer molecules must be minimal so as not to alter the intrinsic polymer properties. However, a recent study utilizing Rutherford backscattering spectroscopy (RBS)[11] to study the interaction between polymer and gold nanoparticles showed that substantial diffusion of gold particles can occur in polymer matrices, a serious problem for interfacial marking applications. The rheological properties of the gold nanoparticles in the polymer matrix, including molecular mobility and viscosity, were found to vary substantially due to interactions between the polymer chains and the metal particles. Factors including particle size, effective cross-linking of polymers, and their interactions at the interface appeared to affect the results.

There have been numerous studies of gold nanocomposites using scattering techniques with focused beams. Such

a)Author to whom correspondence should be addressed; electronic mail: kwshin@kjist.ac.kr
b)Current address: Department of MSE, Michigan Technological University.

techniques are highly surface sensitive due to the large scattering cross sections of the interfaces.[11,14,17–19] Examples of such studies include the use of x-ray reflectivity (XR) to probe the position of the gold particles in a polymer matrix[18] as well as the use of RBS to profile the displacement of gold markers[11,17] already noted. A combined study of x-ray reflection and standing wave fluorescence spectroscopy has also been used to probe small volume fractions of gold nanoparticles inside polymer thin films.[19] However, due to the relatively low resolution (2–8 nm) of the measurements in the noted studies, none permitted detailed analysis of the structure or evolution of the gold nanoparticles themselves.

Sandwiched metallized polymer thin films, where both surfaces of the metallic layer are in contact with polymer layers, permit investigation of the metal-polymer interaction without the complications posed by a free surface. Structures with gold layers of different average thickness between two thin polystyrene (PS) layers were fabricated for this study. X-ray reflectivity was used to quantify both the evolution of the gold nanoparticles into which the gold layers were deposited, or evolved during annealing, as well as the evolution of the polymer/polymer interface. The samples were studied *ex situ* during interrupted anneals.

In this article, a Fourier method for analyzing XR data was used to increase XR sensitivity.[20,21] This technique uses different limits of integration in q space so that interfacial parameters can be determined with high accuracy even when the density profile of the structure being examined is complex. The detailed structure of the gold nanoparticles at the nanoscale was thus monitored, permitting examination of the interaction between the nanoparticles and the polymer matrix. Transmission electron microscopy (TEM) was also used to obtain microstructural information for comparison.

II. EXPERIMENTS

A. Experimental procedure

The two polymers with different molecular weights used in this study are deuterated polystyrene ($M_w/M_n=1.04$), designated as PS_s, of $M_w=52.3$ k and hydrogenated polystyrenes ($M_w/M_n=1.04$) designated as PS_ℓ, of $M_w=168.5$ k.[22] Specimens were fabricated by first spin coating a PS_s layer of approximately 60 nm onto a clean silicon wafer from toluene solution. Next a gold layer of the required average thickness was deposited on top of the first PS_s layer using an electron beam evaporator source. The source material was 99.99% gold in a graphite crucible. The substrates were clamped to a water-cooled block for the deposition, and a deposition rate of ≈ 0.2 nm/s was used. The base vacuum of the system prior to deposition was mid 10^{-6} Pa (10^{-8} Torr) range or better, though pressures in the high 10^{-5} Pa were reached during deposition as the presence of the PS layer precluded use of a pre-bake or pre-deposition step to remove contaminants adsorbed on the surfaces inside the chamber. Five different specimens were fabricated with the average thickness of the gold films (d_{Au}) ranging from 2.5 to 7 nm. Finally, for the top layers, PS_ℓ layers ≈ 70 nm thick were spun onto a clean glass substrate. These films were floated on distilled water and deposited onto the Au/PS_s covered substrate [Fig. 1(a) shows a schematic of the specimens].

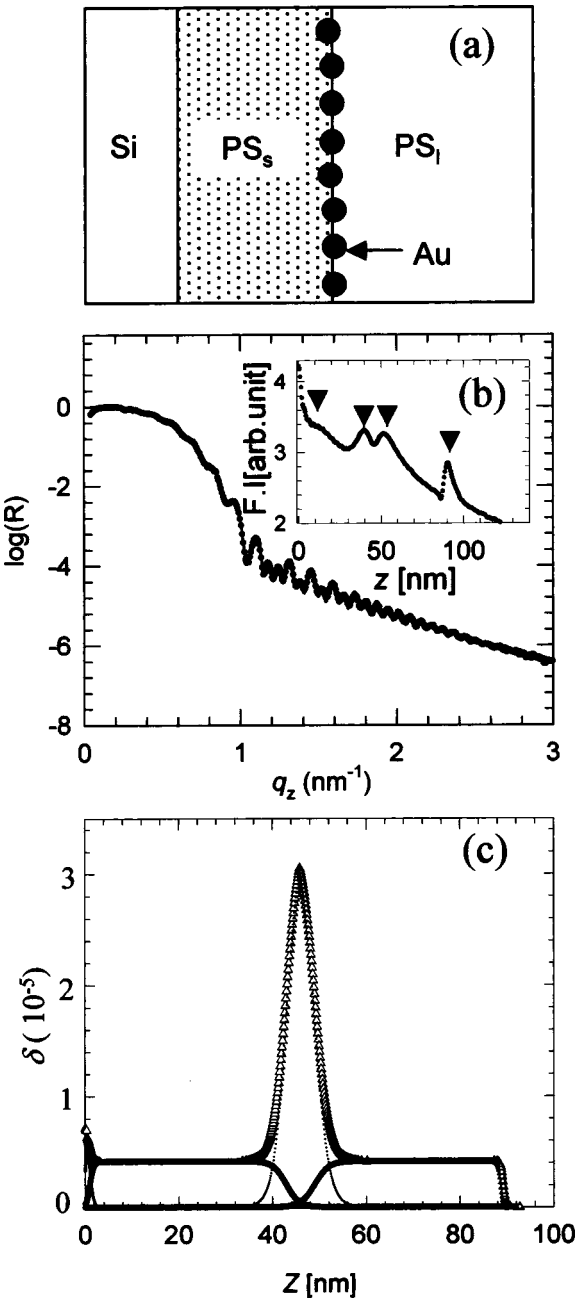

FIG. 1. (a) A schematic structure of a gold layer confined at two polymer thin layers. (b) X-ray reflectivity data of a gold layer confined at two polymer thin layers. The solid line represents the best fits to the experimental data points. Inset: Fourier intensities obtained with a cutoff, $q_{z,\mathrm{low}}=0.95\ \mathrm{nm}^{-1}$ chosen in Fig. 1(b). Arrows in the inset indicate the Fourier peaks from the thicknesses of the gold, PS_s, PS_ℓ, and total layer, respectively (from the left). (c) The open triangles are the total dispersion profile used to obtain the fits in (b). The thick lines indicate respective layer profiles of the PS_s and the PS_ℓ, and dots give the gold profile between the layers.

The geometries of the Au/PS_s structures was characterized by XR prior to addition of the PS_ℓ layer. The full $PS_\ell/Au/PS_s$ structures were also characterized prior to annealing. Subsequent XR studies were conducted by interrupting specimen annealing every 10 min. This time interval is

close to the estimated 700 s reptation time of the bottom layer at the 120 °C annealing temperature, which is higher than the ≈100 °C bulk glass transition temperature. Specimen annealing was done in a vacuum of $\approx 10^{-4}$ Pa.

XR was performed in the standard symmetric reflection geometry using a two-axis reflectometer with a Cu $K\alpha$ source. In this geometry, the scattering wave-vector transfer is given by $q_z = 4\pi/\lambda \sin(\theta)$ and is varied by changing the angle θ between the specimen normal and the incident radiation. The detector, at 2θ, meets the specular condition. The horizontal detector slits were wide open to achieve integration over q_y and the vertical slit in front of the analyzer was set to 0.2 mm defining the q_x and q_z resolutions. Specular scattering is sensitive to variation of the electron density $\rho(z)$ in the direction of the surface normal, averaged in the (x,y)-plane region being studied, making these results sensitive to the layer thickness, density contrast and interfacial roughness.

B. Data analysis procedure

Figure 1(b) shows representative reflectivity data versus q_z from a Au film of 5.7 nm average thickness sandwiched between a 60-nm-thick PS_ℓ layer and a 40-nm-thick PS_s layer on the silicon substrate. This sample was annealed for 120 min at 120 °C. The solid line in the figure is the fit calculated by the Parratt algorithm[23] with the modeled density profile in the region of the gold layer optimized to fit the experimental data (and assuming oxide-covered Si). The fit has been obtained as follows. The dispersion δ is expressed in terms of the electron density ρ_{el} using $\delta = \lambda^2 \rho_{el} r_o / 2\pi$ where r_o is the classical electron radius (2.82×10^{-13} cm^{-13}), the wavelength λ is (0.155 nm) for 8 keV from Cu $K\alpha$ and ρ_{el} is the electron density of the material. Neglecting absorption, the indices of refraction $n \equiv 1 - \delta$ are $n_{Au} = 1 - 4.773 \times 10^{-5}$ (using $\rho_{el} = 4.418 \times 10^3$ e$^-$/nm^3) and $n_{PS} = 1 - 3.602 \times 10^{-6}$ (using $\rho_{el} = 3.34 \times 10^2$ e$^-$/nm^3) for Au and PS, respectively. In fitting the scattering data, the electron density (equivalently the dispersion δ) at each interface was modeled as a hyperbolic tangent function having a probability density with rms roughness consistent with variation of the layer thickness within the plane of the specimen.[24]

As Reiter *et al.*[18] pointed out, the overall reflectivity of Au embedded systems is often dominated by a high reflectance from the Au-PS_ℓ interface. Thus, the underlying information, especially from the bottom PS layer (PS_s) is often considered insignificant and ignored. To overcome this problem, we used an analysis that helps to amplify the intensity from weakly scattering interfaces during the fitting process. In Fig. 1(b), the sandwiched Au layer with ~50% coverage produces a complex interference pattern with several correlated frequencies arising from the thicknesses of the top layer (PS_ℓ), bottom layer (PS_s), combined polymer and gold layers (PS_ℓ + Au and Au + PS_s), and total thickness (PS_ℓ + Au + PS_s). To enhance the signals from these interfaces, we take the Fourier back transformation (FBT) of the scattering intensity, $I(q_z)$, as introduced by Seeck *et al.*[20] Following the Fourier method described in Ref. 20, the Fourier intensity (F) is given by, $F(d, q_{z,low}) = |\int_{q_{z,low}}^{q_{z,up}} q_z^4 \hat{I}(q_z) \exp(iq_z d) dq_z|^2$, where d is distance from the substrate in real space. In this case each layer gives a unique peak in the $I(d)$ phase space. The shape of the peaks becomes a sensitive function of the interfacial widths, the ratio of the roughnesses and the low q_z cutoff, $q_{z,low}$. In addition, this method allows one to differentiate between the roughnesses at the Au/PS_ℓ interface and at the two Au/PS_s interfaces. In particular, as $q_{z,low}$, is increased, the amplitude of the peak corresponding to the rougher of the interfaces decreases. The positions of the two interfaces are readily distinguished by their d values. An example data set, which is Fourier transformed with a cutoff, $q_{z,low} = 0.95$ nm^{-1} indicated in Fig. 1(b), is shown in the inset to Fig. 1(b). The four peaks corresponding to the gold, PS_s, PS_ℓ and total film thicknesses are evident. Small changes at the interfaces can be more readily resolved by fitting this Fourier transformation (FT) curve simultaneously with the entirety of the untransformed XR data. In this study, fits to the reflectivity data were done using this FT method, where three FTs with different $q_{z,low}$ arbitrarily were used in a χ^2 minimization process. Figure 1(c) shows the δ profile, as a function of distance z from the Si surface that was used to fit the reflectivity data. More detailed descriptions of the data analysis technique can be found in the literature.[20,21]

III. RESULTS AND DISCUSSION

A. Experimental data and modeling results

Figures 2(a)–2(c) show the XR data from three representative specimens. They differ only in the thicknesses of the gold layers. The solid lines are the fits obtained from the corresponding volume fraction profiles, consisting of a high-density region of gold in the middle and two low-density regions of PS on either side. Each layer is modeled using three adjustable fitting parameters: thickness (d), electron density (ρ_{el}) and roughness (ρ) for the interface between that layer and the next layer away from the Si substrate. Figures 3(a)–3(c) show the distribution of the gold corresponding to the fits of Figs. 2(a)–2(c), respectively, as a volume fraction ϕ_{Au}, which equals $\rho_{el}(z)/\rho_{Au}$, where ρ_{Au} is the electron density of bulk gold at an incident energy of 8 keV (4.418×10^3 e$^-$/nm^3) along the surface normal. The detailed fitting parameters used are listed in Table I.

Figure 2(a) shows specular reflectivity data for the specimen with the thinnest Au layer at accumulated annealing times $t = 0$, 30 and 240 min (from the top). Length scales and composition profiles were obtained by fitting the scattering data. A pronounced low frequency oscillation, with a first minimum at $q_z \approx 2.1$ nm^{-1}, indicates that the average thickness of the gold layer prior to annealing is $d_{Au} \approx 2.9$ nm with relatively sharp interfaces of 0.8 and 0.7 nm for the PS_s/Au and Au/PS_ℓ interfaces, respectively; the solid circles in Fig. 3(a) give the corresponding Au profile. The maximum area fraction of Au, occurring essentially at the midplane of the Au layer, is $\phi_{Au} \approx 0.45$. This indicates formation of a non-continuous structure within the Au layer. Two oscillations with higher frequencies arise from the thickness of the PS films; beating is visible in the signal because the frequencies are similar. The small amplitude oscillation at the highest frequency arises from the thickness of the entire layered struc-

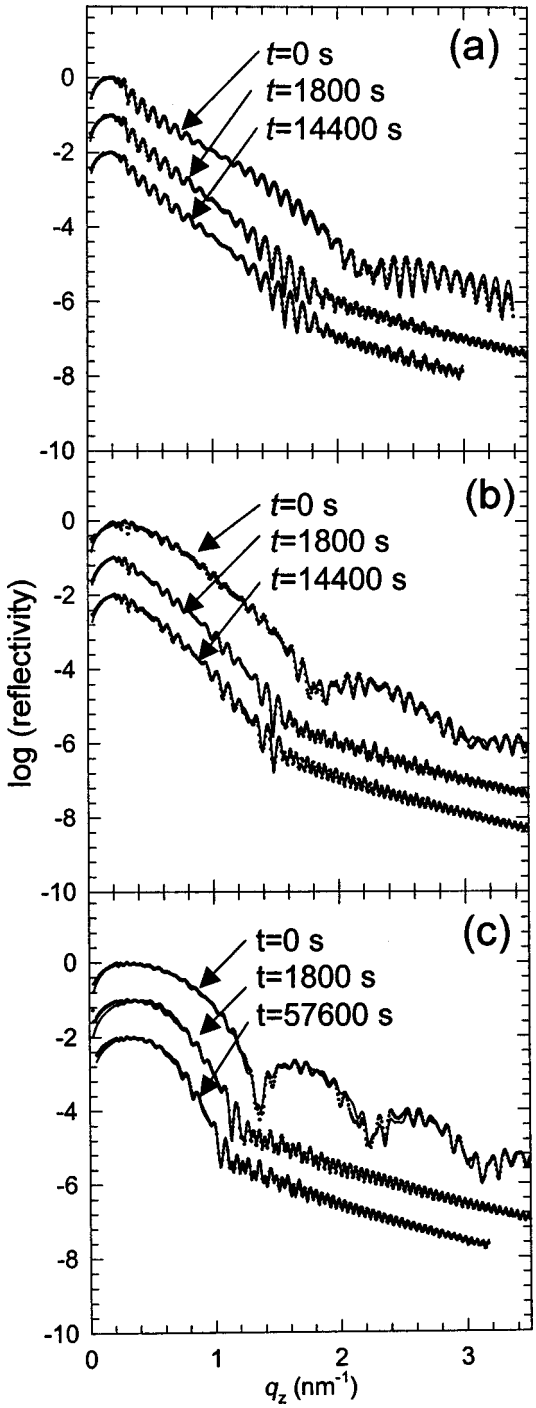

FIG. 2. X-ray reflectivity data of gold layers with various thicknesses confined between two PS layers, (a) $d=2.9$ nm, (b) $d=3.7$ nm and (c) $d=5.7$ nm at indicated annealing times. The solid curves are fits, with data for different annealing times offset vertically for easier viewing.

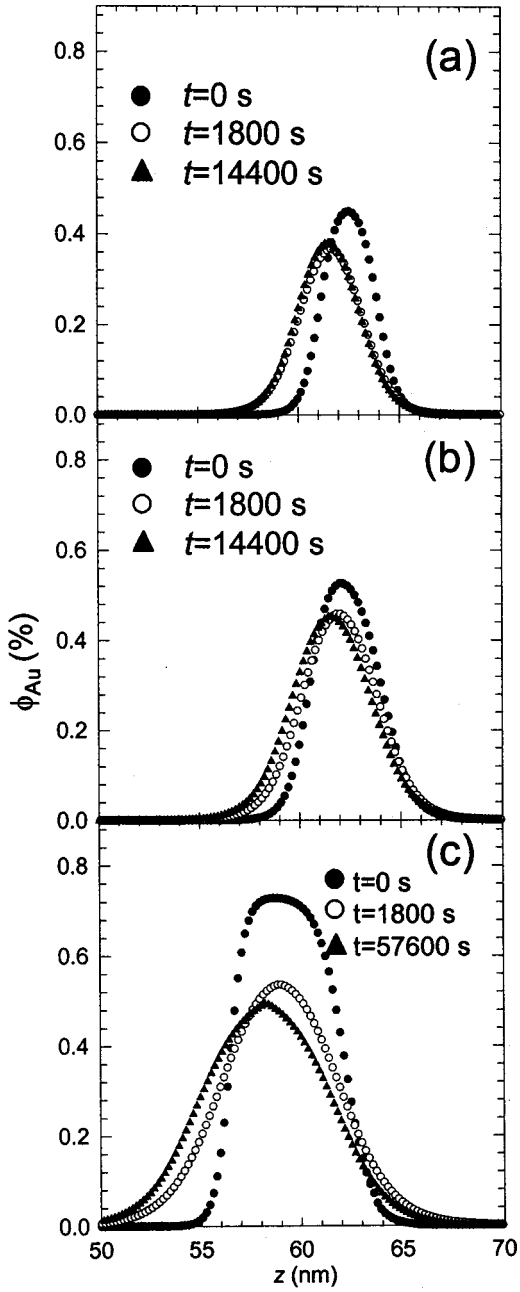

FIG. 3. The Au volume fractions of gold layers with various thicknesses (a) $d=2.9$ nm, (b) $d=3.7$ nm and (c) $d=5.7$ nm confined between two PS layers, at indicated annealing times are obtained from the fits of Figs. 2(a)–2(c), respectively. The distance z is relative to the substrate.

ture. Figures 2(b) and 2(c) show the reflectivity profiles obtained from specimens with thicker Au layers. The low frequency oscillations are more pronounced, indicating sharper interfaces, and the Kiessig fringes are at higher frequencies. The Au distributions obtained from fitting the data are shown in Figs. 3(b) and 3(c). The average Au layer thicknesses are 3.7 and 5.7 nm, respectively, with higher maximum area coverages, $\phi_{Au}=0.55$ and $\phi_{Au}=0.75$.

After annealing for 30 min at 120 °C, the low frequency oscillation essentially disappears from the reflectivity profile of the specimen with $d_{Au}\approx 2.9$ nm [Fig. 2(a)]. The loss of this signal indicates broadening of the metal-polymer interfaces due to decreased sharpness of the interfaces. This broadening arises from deformation of the gold layers as broadening by interdiffusion is not possible for the Au-PS system. The open circles in Fig. 3(a) show the corresponding Au distribution obtained from analysis of the XR data. The interface roughnesses $\sigma_{PS_s\text{-}Au}$ and $\sigma_{PS_\ell\text{-}Au}$ have increased,[25] the volume fraction of gold at the midplane of the gold layer has decreased slightly, and the region containing the gold particles has thickened (see Table I). The center of the gold

TABLE I. Electron densities and thicknesses obtained from the specular reflectivity data fits. The typical errors of the thickness are 0.1–0.2 nm. The errors of the electron densities and roughnesses are 5% and 10% of the value, respectively.

	PS_s		Au					PS_ℓ		
t (min)	d_{PS_s} (nm)	δ_{PS_s} (nm)	$\sigma_{PS_s\text{-Au}}$ (nm)	d_{Au} (nm)	δ_{Au} (nm)	ϕ_{Au}	$\sigma_{PS_\ell\text{-Au}}$ (nm)	d_{PS_ℓ} (nm)	δ_{PS_ℓ} (nm)	σ_{PS_ℓ}-air (nm)
					Parameters for Fig. 2(a)					
0	60.7	0.36	0.8	2.9	2.20	0.46	0.7	67.7	0.36	0.5
30	59.6	0.36	1.4	2.9	2.14	0.45	1.3	66.4	0.36	0.7
240	59.5	0.36	1.3	2.9	2.17	0.45	1.3	66.2	0.36	0.7
					Parameters for Fig. 2(b)					
0	59.9	0.36	0.7	3.6	2.63	0.55	1.1	74.9	0.36	0.6
30	59.3	0.36	1.9	3.7	2.57	0.55	2.2	74.9	0.36	0.6
240	59.1	0.36	1.8	3.8	2.59	0.54	1.9	74.7	0.36	0.5
					Parameters for Fig. 2(c)					
0	56.1	0.36	0.8	5.7	3.29	0.73	1.1	75.9	0.36	0.7
30	55.7	0.36	2.4	5.7	2.90	0.60	2.2	75.8	0.36	0.7
960	54.7	0.36	2.6	6.0	2.50	0.52	2.2	76.2	0.36	0.7

layer has also moved toward the substrate during the annealing as indicated by the 1.1 nm decrease of the PS_s layer thickness. Subsequent change of the profile during further annealing for a total of 240 min is minimal, implying that equilibrium of this system has been reached during the first 30 min of annealing (ignoring the much slower coarsening of the ensemble of gold particles and interdiffusion of the PS layers).

The other specimens behaved similarly. After 1800 s (30 min) of annealing the low frequency oscillations disappeared [Figs. 2(b) and 2(c)] and the gold layers shifted in the low-M_w polymer (PS_s) direction by 0.6 and 0.4 nm [Figs. 3(b) and 3(c), respectively]. Figure 4 summarizes the data on displacements of the Au layers for these three specimens. The majority of the displacement occurs within the first 30 min of annealing. More work is in progress to investigate if there is a net flux of polymer across the gold layer during longer anneals. If there is, and it is controlled by diffusion of the low-M_w polymer, diffusion coefficient D_s, then displacement of the Au layer with time t is expected to be proportional to $(D_s t)^{1/2}$.[17,18] This deformation was observed only when the Au layer was confined between two PS layers. No comparable change in the Au layer was observed even after 10 h at 160 °C in the absence of the top PS layer.

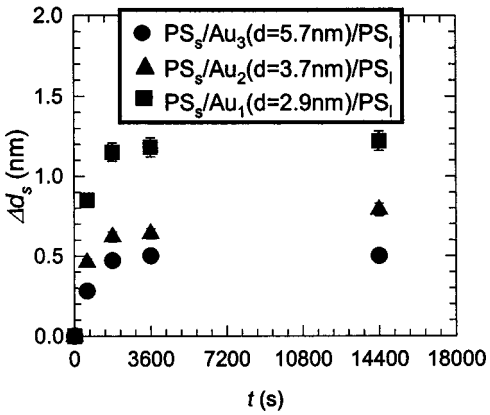

FIG. 4. Time dependence of the displacement distance of Au layers between PS layers for specimens with $d=2.9$ nm (squares), $d=3.7$ nm (triangles) and $d=5.7$ nm (circles).

Because the structural evolution is related to the motion of both gold atoms and polymer molecules along the interfaces, one might expect the slower process to limit the deformation. The motion of polymers in the melt can be described in terms of a reptation model that predicts the period of time required for a polymer chain to diffuse out of its contour. The reptation time τ_{PS_s} of PS_s layer ($M_w = 52.3$ kg/mol) at 120 °C is 700 s; this is significantly shorter than the reptation time $\tau_{PS_\ell} = 23\,600$ s of PS_ℓ ($M_w = 168.5$ kg/mol) at this temperature. In light of the relatively large reptation time of the PS_ℓ, the substantial morphological deformation obtained at the Au/PS_ℓ interface during the 30 min anneals would seem unexpected. The time dependence of the detailed profiles will be discussed later.

B. Interpretation of XR results

The low maximum area coverages ϕ_{Au} for the non-annealed samples, e.g., $<50\%$ of bulk value for $d_{Au} \approx 2.9$ nm [Figs. 3(a)–3(c)], are consistent with preexisting intercalation of the polymer matrix and gold nanoparticles. The apparent decrease of the gold volume fraction ϕ_{Au} at the midplane during annealing is consistent with Au moving away from the midplane during spheroidization of initially "flat" gold particles due to capillary driving forces (interface free energy minimization). The decrease of the PS_s layer thicknesses, indicating penetration of additional low-M_w polymer into the gold layers during this process, might be associated with such a change in particle shape or migration of the Au particles into the low-M_w polymer to further reduce interfacial energy. The relatively constant thickness of the PS_ℓ layers throughout the annealing process indicates minimal deformation of the high-M_w polymer, appropriate for its higher viscosity (the diffusion coefficient of the upper layer with $M_w = 168$ k is expected to be at least ten times smaller (1.0×10^{-17} cm^2/s) than that of the bottom layer (1.1×10^{-16} cm^2/s) with $M_w = 52$ k at 120 °C).[17]

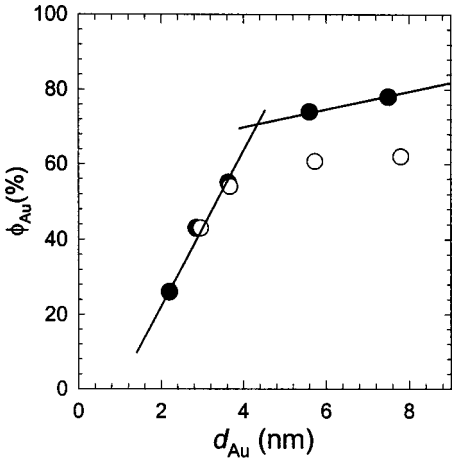

FIG. 5. Volume fraction vs thickness of the condensed gold layers, before annealing (solid circles) and after annealing (open circles). The solid lines are used only to guide the eye to the transition region at about 4.0 nm.

C. Discussion of midplane Au coverage results

An atomic force microscope topography image (data is not shown in this article) of the 5.4-nm-thick Au film deposited on PS_s surface indicates that a smooth surface has been formed. No sign of discontinuous gold films was observed. Therefore, a continuous layer structure, prior to annealing, is suggested at this thickness, in contrast to the layers with $d_{Au}<4$ nm. The maximum fraction ϕ_{Au} of Au for the nonannealed samples (essentially the value at the midplane) is plotted against the average Au thickness d_{Au} in Fig. 5 (solid circles). The maximum fraction ϕ_{Au} changes rapidly with d_{Au} from 2 to 4 nm then changes less rapidly for thicker Au layers. This result implies a change in the morphology of the deposited Au layers occurs by approximately 4 nm of Au deposition. It is proposed here that the morphology change is substantial impingement of Au particles that are isolated in thinner Au layers.

The open circles in Fig. 5 represent the ϕ_{Au} of the gold layers in samples after 240 min of annealing. From the figure, for $d_{Au}<4$ nm, the values are very close to those for the nonannealed samples, indicating no significant morphological change of the Au particles during annealing. In contrast, for $d_{Au}>4$ nm, the volume fractions at the center of the Au layer decrease significantly during annealing. Both these results are consistent with the existence of isolated particles for the thinner layers and significantly impinged particles in the thicker layers proposed above.

Figure 6(a) depicts the time dependence during annealing of the normalized maximum density of the gold for all three specimens. After 30 min of annealing, the gold densities reached an equilibrium state, with the PS molecules occupying the interstitial volume. Assuming that the clusters are spherical with an average diameter, the morphological structures, including the size of the gold clusters and the inter-cluster distance, can be estimated. Specifically, if the particles are spheres (either as deposited or after annealing-induced spheroidization), the Au particle radius r_{Au}, the particle spacing a, and the average Au thickness d are related by

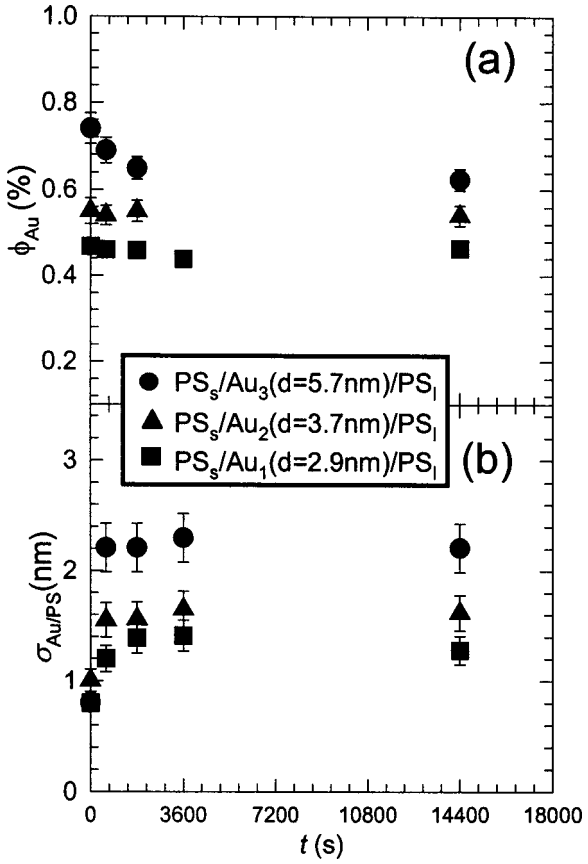

FIG. 6. Time dependence of (a) the maximum volume fraction of the gold layers, and (b) the average roughnesses of $\sigma_{PS_s\text{-}Au}$ and $\sigma_{PS_\ell\text{-}Au}$ obtained for specimens with $d=2.9$ nm (squares), $d=3.7$ nm (triangles) and $d=5.7$ nm (circles). The errors of the volume fractions and roughnesses are 5% and 10% of the value, respectively.

$$\tfrac{4}{3}\pi r_{Au}^3 = d a^2. \tag{1}$$

This will apply until impingement of adjacent particles occurs for

$$2r_{crit} = a. \tag{2}$$

From these two relationships, one immediately obtains

$$d_{crit} = \frac{\pi}{6} a \tag{3}$$

as the Au layer thickness at which impingement is predicted to occur. From the micrograph in Fig. 7(b), a is equal to approximately 15 nm *after* breakdown of the connected structure (value for a square array using the 112 particles visible in the 256 nm^2 area of the micrograph). Specimens with $d_{Au}>d_{crit}$ would be expected to possess significant particle impingement. A corresponding decrease of ϕ_{Au} upon annealing of these specimens in particular would also be expected. It is straightforward to predict the functional form of ϕ_{Au} versus film thickness d_{Au} using Eq. (1), with the particle spacing a obtained from TEM results, for the films where impingement is not significant ($d_{Au}<d_{crit}$) and a form that accounts for overlap once impingement occurs.

When Au coverage of the PS_s surface is discontinuous, spheroidization involves only the rounding of the mass within the original, already circular in cross section, particle.

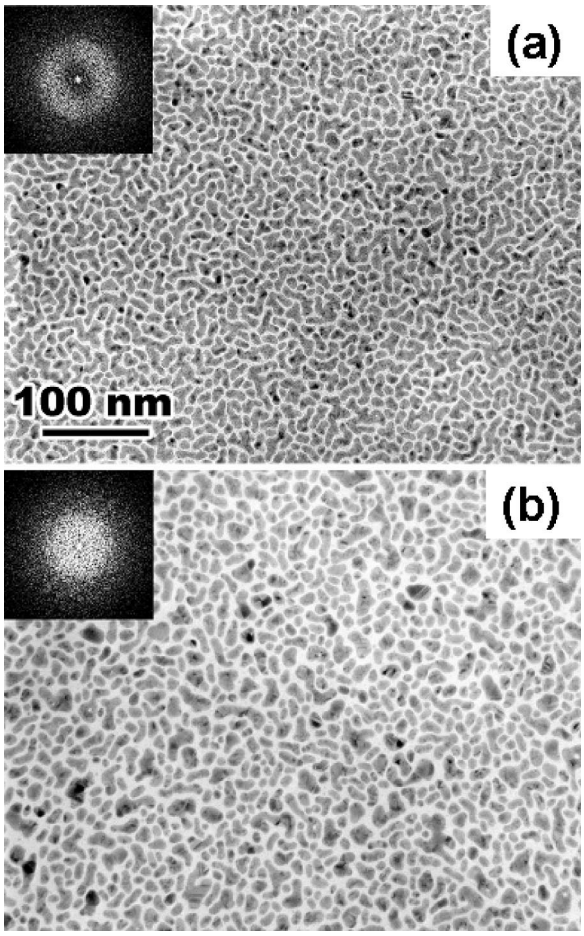

FIG. 7. Transmission electron micrograph of $PS_s/Au_3(d=5.7\ nm)/PS_\ell$ film (a) before and (b) after annealing for 6000 s. Insets are the FFTs of the corresponding TEM data. Note that the floating procedure requires the specimens to contact boiling basic water.

The fact that the rapid deformation of the interfaces occurs only for Au layers more than 4 nm thick, where connectivity of the Au particles in the unannealed specimen is evident, is consistent with this proposed mechanism. The reduced connectivity and more circular cross sections of the Au particles in the annealed specimens, consistent with spherical particles, are also consistent. These results show that the deformation process of Au layers confined between PS layers is highly dependent on the average layer thickness for values up to 6 nm.

The deformation process can be further analyzed by comparing the roughness σ obtained from fitting the specular reflectivity. The values of obtained for different samples are compared as functions of annealing time in Fig 6(b) where the average values of $\sigma_{PS_s\text{-}Au}$ and $\sigma_{PS_\ell\text{-}Au}$ obtained are shown. The growth of roughness will begin as the Au particles spheroidize and separate, with associated diffusion of PS molecules into the inter-cluster area. From the figure, it is evident that, in contrast to the two thinner Au layers, a rapid broadening of occurs after 10 min of annealing for the thickest Au sample.

D. Transmission electron microscopy

Structural information for the specimens was also obtained using planview TEM. The sandwiched Au films were floated off the oxide-covered silicon substrates by immersion in a boiling NaOH solution after which they were lifted directly onto TEM grids for study in the microscope. The average Au particle size and geometry, as well as the interparticle spacing in the polymer matrix, were then determined from scanned negatives using the UTHSCSA ImageTool.[26] Figures 7(a) and 6(b) are planview TEM micrographs from the specimen with $d_{Au}\approx 5.7$ nm before (a) and after (b) annealing for 100 min at 120 °C, respectively. The Au particles appear as the darker regions. Note that, because of the TEM specimen fabrication procedure, even the pre-anneal specimens do not necessarily possess the true as-deposited microstructure. Nonetheless, comparison of the pre-anneal and postanneal specimens is still instructive.

From Fig. 7(a), the gold layer exhibits a thickness modulation with a well-defined width and a fairly broad range of lengths. The characteristic wavelengths in the gold morphology can be quantified by fast Fourier transform (FFT) of the figure, where it gives rise to the ring pattern of intensity [inset to Fig. 7(a)]. The inner diameter of the ring corresponds to the average long dimension of the particles, and the outer diameter to the average short dimension. Using UTHSCSA ImageTool, values of 19 ± 10 and 9 ± 4 nm are obtained for the long dimension and the short dimension, respectively. That the FFT is radially symmetric indicates a random orientation of the pattern in the plane of the interface.

Comparison of Figs. 7(a) and 7(b) shows that increased annealing leads to a spherical shape for the gold particles. The diameter of the ring in the FFT indicates the average diameter of the particles while the breadth of the ring arises from the range of particle sizes and spacings. These presumably result from the stochastic nature of the coarsening and breakup from the elongated random structure visible prior to the annealing. The fractional area covered with Au obtained from the TEM images is in good agreement with the x-ray data (in Fig. 5).

IV. CONCLUSION

We have used XR to measure the morphological profiles of thin Au layers of three different average thicknesses sandwiched between two polystyrene layers with different molecular weights, $M_w=52.3$ k and $M_w=168.5$ k. The results showed that the equilibrium structures of the samples with the thinnest layers ($d_{Au}<4$ nm), where discontinuous islands are expected, were very close to those of the nonannealed samples. Annealing of specimens $d_{Au}>4$ nm, where a continuous layer structure was formed, resulted in deformation of the Au layers. This occurred in a period of time that was relatively short compared to the reptation times of the more viscous of the polymer matrices. Comparison of the TEM micrographs from the before and after annealed samples showed that increased annealing leads to a spherical shape for the Au particles from the stochastic nature of the coarsening and breakup from the elongated random structure visible prior to the annealing. The fractional area covered with Au obtained from the TEM images is in good agreement

with the x-ray data. These results were interpreted in terms of capillarity induced spheroidization of the ultrathin Au layers.

ACKNOWLEDGMENTS

Throughout this analysis, K. S. used the fitting routine written by Dr. O. H. Seeck at HASYLAB, Germany. Part of this work was supported by the Ministry of Science and Technology of Korea through Proton Accelerator User Program (No. M102KS010001-02K1901-01810) of Proton Engineering R&D Project from the Nuclear R&D Program and the 21st Century Frontier R&D Program.

[1] R. L. Whetten, M. N. Shafigullin, J. T. Khoury, T. G. Schaaff, I. Vezmar, M. M. Alvarez, and A. Wilkinson, Acc. Chem. Res. **32**, 397 (1999), and references therein.
[2] A. C. Templeton, W. P. Wuelfing, and R. W. Murray, Acc. Chem. Res. **33**, 27 (2000), and references therein.
[3] E. Hedborg, F. Winquist, and I. Lundstr̃om, Appl. Phys. Lett. **64**, 420 (1994).
[4] *Metallized Plastics: Fundamentals and Application*, edited by K. L. Mittal (Dekker, New York, 1998).
[5] T. L. Morkved, P. Wiltzius, H. M. Jaeger, D. G. Grier, and T. A. Witten, Appl. Phys. Lett. **64**, 422 (1994).
[6] R. W. Zehner, W. A. Lopes, T. L. Morkved, H. Jaeger, and L. R. Sita, Langmuir **14**, 241 (1998).
[7] MRS Bull. **22**, (1997).
[8] R. D. Miller, J. L. Hedrick, D. Y. Yoon, R. F. Cook, and J. P. Hummel, MRS Bull. **22**, 44 (1997).
[9] R. R. Tummala, R. W. Keyes, W. D. Grobman, and S. Kapur, in *Microelectronics Packaging Handbook*, edited by R. R. Tummala and E. J. Rymaszewski (Van Nostrand Reinhold, 1989), p. 673.
[10] J. Bischof, D. Scherer, S. Herminghaus, and P. Leiderer, Phys. Rev. Lett. **77**, 1536 (1996).
[11] D. H. Cole, K. R. Shull, L. E. Rehn, and P. Baldo, Phys. Rev. Lett. **78**, 5006 (1997).
[12] J. Wang, M. Tolan, O. H. Seeck, S. K. Sinha, O. Bahr, M. H. Rafailovich, and J. Sokolov, Phys. Rev. Lett. **83**, 564 (1999).
[13] M. S. Kunz, K. R. Shull, and A. J. Kellock, J. Appl. Phys. **72**, 4458 (1992).
[14] R. Weber, K.-M. Zimmermann, M. Tolan, J. Stettner, W. Press, O. H. Seeck, J. Erichsen, V. Zaporojtchenko, T. Strunskus, and F. Faupel, Phys. Rev. E **64**, 061508 (2001).
[15] F. Faupel, V. Zaporojtchenko, T. Strunskus, J. Erichsen, K. Dolgner, A. Thran, and M. Kiene, Workshop on Polymer Metallization, Montreal 2001, and references therein.
[16] A. Thran, M. Kiene, V. Zaporojtchenko, and F. Faupel, Phys. Rev. Lett. **82**, 1903 (1999).
[17] P. F. Green, C. J. Palmstrøm, J. W. Mayer, and E. J. Kramer, Macromolecules **18**, 501 (1985).
[18] G. Reiter, S. Hüttenbach, M. Foster, and M. Stamm, Macromolecules **24**, 1179 (1991).
[19] B. Lin, T. L. Morkved, M. Meron, Z. Huang, P. J. Viccaro, H. M. Jaeger, S. M. Williams, and M. L. Schlossman, J. Appl. Phys. **85**, 3180 (1999).
[20] O. H. Seeck, I. D. Kaendler, M. Tolan, K. Shin, M. H. Rafailovich, J. Sokolov, and R. Kolb, Appl. Phys. Lett. **76**, 2713 (2000).
[21] K. Shin, H. Wang, S. K. Satija, C. C. Han, D. Jossell, Mater. Res. Soc. Symp. Proc. **710**, DD14.7 (2001).
[22] The use of both hydrogenated and deuterated PS gives high contrast between the different PS layers for neutron reflection. This has permitted study of the interdiffusion dynamics. A quantitative analysis of the interdiffusion at the gold nanoparticle interface will be published separately.
[23] L. G. Parratt, Phys. Rev. **95**, 359 (1954).
[24] T. P. Russell, Mater. Sci. Rep. **5**, 171 (1990).
[25] Reasonable fits over the entire q range required inclusion of a low-density layer of 1.5 nm thickness at the PS/Au interface consistent with an air gap incorporated during the floating process. This low-density layer disappeared after the annealing process.
[26] Identification of a commercial product does not imply endorsement by the National Institute of Standards and Technology.